Computational Geosciences (2021) 25:2131–2147
https://doi.org/10.1007/s10596-021-10082-x

ORIGINAL PAPER

High performance computing of 3D reactive multiphase flow in porous media: application to geological storage of CO_2

Etienne Ahusborde[1] · **Brahim Amaziane**[1] · **Mohamed Id Moulay**[2]

Received: 24 August 2020 / Accepted: 21 July 2021 / Published online: 24 August 2021

Abstract

In this paper, we formulate and test numerically a fully coupled fully implicit finite volume (FV) method for solving the nonlinear coupling between two-phase flows and geochemical reactions in porous media on a reservoir scale. The problem is modeled by a highly nonlinear system of degenerate partial differential equations (PDEs governing a compositional two-phase flow model) coupled to ordinary and/or algebraic differential equations (modeling kinetic and equilibrium chemical reactions respectively). The spatial discretization uses a cell-centered FV scheme. After discretizing in time with an implicit Euler scheme, the resulting systems of nonlinear algebraic equations are solved with Newton's method and the systems of linear equations are solved efficiently and in parallel with an algebraic multigrid method. We discuss two strategies for selecting local time steps. We have developed and implemented this scheme in a new module in the context of the parallel open source platform DuMu^X. Parallelization is carried out using the DUNE parallel library package. Two numerical experiments are presented to demonstrate the effectiveness and efficiency of the proposed solver for 3D problems modeling scenarios of CO_2 geological storage into a deep saline aquifer. We also report the parallel scalability of the proposed algorithm on a supercomputer with up to 768 processor cores. The proposed method is accurate, numerically robust and exhibits the potential for tackling realistic problems. Lastly, a comparison with a sequential method consisting in decoupling the original problem into a two-phase flow and a reactive transport problem, is performed in term of accuracy.

Keywords Two-phase reactive transport · Porous media · High performance computing · Fully implicit method · DuMu^X · CO_2 geological storage

1 Introduction

Reactive transport modeling is used in a wide range of subsurface applications such as hydrocarbon reservoir production, groundwater management, carbon dioxide sequestration, management of nuclear waste repositories or geothermal energy production. Reference is made to the books [41] or [43] for a detailed overview of the applications of reactive transport models. In this work we focus on Carbon Capture and Storage (CCS). Carbon dioxide (CO_2) is the most important greenhouse gas (74% of human activity). One of the impact factors of recent global warming is the increase in its concentration in the Earth atmosphere. Geological storage of part of the CO_2 emitted is one of the tools considered in the approach to mitigate global warming. The latter is injected in gaseous or supercritical form, into formations such as depleted hydrocarbon reservoirs or confined or very slowly circulating saline aquifers. The whole process is performed by overlapping physical and chemical trapping processes during the storage period [30]. Various geochemical and physical interactions can occur between chemical species and the host rock causing deformations with possible dissolved transport in fractures. The numerical simulation of CO_2 storage allows to forecast the behavior of the CO_2 and its migration into the reservoir due to geophysical phenomena, on time scales ranging from about ten years to thousands of years.

✉ Brahim Amaziane
brahim.amaziane@univ-pau.fr

Etienne Ahusborde
etienne.ahusborde@univ-pau.fr

Mohamed Id Moulay
mohamed.idmoulay@toulouse-inp.fr

[1] Universite de Pau et des Pays de l'Adour, E2S UPPA, CNRS, LMAP, Pau, France

[2] Institut de Mécanique des Fluides de Toulouse (IMFT), Université de Toulouse, CNRS-INPT-UPS, Toulouse, France

Research on numerical simulation of reactive transport models in porous media has evolved considerably in recent decades. Many approaches have been proposed in this framework for solving this type of problems. Such problems are governed by a set of degenerate nonlinear PDEs modeling a compositional two-phase flow coupled to ordinary differential equations (ODEs) and/or algebraic equations modeling respectively kinetic and equilibrium reactions. For the PDEs, besides the nonlinearity due to chemical reactions, there are additional nonlinearities and possible degeneracy due to terms containing relative permeabilities or capillary pressure and when a phase appears or disappears.

The numerical strategies for solving this system can be divided into two dominant algorithms: the global implicit and the sequential approaches [37]. In the global implicit approaches (GIA), one nonlinear system gathering all equations governing multiphase reactive flows is solved at each time step. For the sequential solution approaches, multiphase flow and reactive transport (or possibly, two-phase flow, transport and chemistry) are solved sequentially at each time step, possibly in an iterative loop. For the reactive transport sub-problem, the solution of the transport and chemistry can be either coupled or decoupled, depending on the formulation. In comparison with GIA, sequential approaches can be easier to implement since existing codes and specific methods can be used for each sub-problem (two-phase flow, transport, chemistry). In sequential approaches, the time step is restricted by the famous Courant–Friedrichs–Lewy (CFL) condition to ensure stability. This condition is usually very restrictive in reservoir-scale models, and it is therefore more common to use implicit schemes. Furthermore, sequential approaches introduce operator splitting errors and restrictions on the time step are mandatory to ensure mass conservation for instance [8]. Implicit discretizations capable of taking large(r) time steps are therefore often preferred in practical computations.

The numerical modeling of reactive single phase flow in porous media has been a problem of interest for many years and many fully implicit methods have been developed. Since the pioneering works of [36], there is an extensive literature on this subject. We will not attempt an exhaustive literature review here, but merely mention a few references as for instance [20] or [27]. Some benchmarks exist for reactive single phase flow and several models have been presented in the literature. For instance, in the framework of the MoMaS benchmark proposed in [13], several implicit algorithms have been used. In [6], the authors propose a method where the chemical problem is eliminated locally, leading to a nonlinear system where the transport and chemistry subsystems remain separated. In [16], the problem is written in the form of differential algebraic equations (DAE). In [21], the author use a reduction technique introduced in [25] that aims at reducing the number of coupled nonlinear differential equations drastically. In [28], a direct substitution approach (DSA) consisting in substituting the equations of chemistry directly in the equations of transport is employed. The situation is quite different for reactive two-phase flow in porous media. Indeed, most of the codes presented in [35] and [43] use a sequential approach to deal with the strong nonlinear coupling between multiphase flow and reactive transport. However, let us note that some new fully implicit codes for multiphase reactive flows emerged in the last decades, see for instance [12, 18, 22, 29] and the references therein.

In [5] we developed a fully implicit approach to deal with reactive two-phase flows. We validated our methodology, by considering a 1D test case proposed in [32]. Despite its relatively simple geometry, this test case presented the additional difficulty to deal with porosity and permeability changes. This contribution aims at extending this fully implicit strategy to 2D and 3D configurations using HPC tools and at comparing fully implicit and sequential strategies in the same numerical environment. Examination of the existing literature shows a clear trend in evaluating the efficiency of the different algorithms through calculations performed on different environments or computer facilities.

Despite the intensive research carried out in recent years, the solution to reactive multiphase equations still represents a challenging and computationally demanding task. The overall objective of this research is the development of a new-generation framework and simulator suitable for massively parallel processors. The next generation of reservoir simulators may need, at least, to be able to run high-resolution reservoir studies on the order of a million grid-blocks; to model complex physical processes in a realistic manner; and to perform numerical simulation efficiently.

The rest of the paper is organized as follows. In Section 2, we describe the governing equations for a two-phase multicomponent flow with reactive transport. In Section 3, our fully implicit strategy is detailed and its discretization using a FV scheme is presented. We first describe the DSA formulation followed by the FV scheme. In Section 4, a description of the implementation of our strategy in DuMu^X [14, 24] is given and some specific optimizations concerning the time step are detailed. Then, to validate our approach, we consider two 3D test cases, for which numerical results are exhibited by comparison with published results. Finally, some concluding remarks and perspectives are presented in Section 5.

2 Mathematical formulation of the problem

In this section, we present the geochemical and mathematical models for two-phase multicomponent flow with

reactive transport in porous media. We limited ourselves to two-phase flows (liquid-gas) with phase exchange, but our study can be extended to a general framework of compositional multiphase flows. For a general discussion on the physical principles of the multiphase reactive flows in porous media, we refer e.g. to [33] while for a detailed description of geochemical reaction modeling, we refer e.g. to [9]. We recall here the basic facts and notations to be used in this paper. In the sequel, the index $\alpha \in \{aq, g, s\}$ (aq for aqueous, g for gas and s for solid) stands for the phase, while the superscript i refers to the component.

2.1 Geochemical model

We adopt here the same notations as in [5]. The only difference is that in the present article, we also consider kinetic reactions. Precisely, I denotes the set of all N_c chemical components involved in the N_r chemical reactions. Adopting the Morel formalism, we split these components into primary and secondary components (each secondary component can be formed as a set of the primary ones) that are noted respectively I_p and I_s such that $I = I_p \cup I_s$. The set of primary components I_p is then divided into mobile primary components I_{pm} and immobile primary components I_{pi} such that $I_p = I_{pm} \cup I_{pi}$. Likewise, the set of secondary components I_s is decomposed into mobile secondary components I_{sm}, immobile secondary components I_{si}, components involved in equilibrium dissolution/precipitation reactions I_{se}, and components involved in kinetic reactions I_{sk} ($I_s = I_{sm} \cup I_{si} \cup I_{se} \cup I_{sk}$). $N_{re} = \text{card}\{I_{sm} \cup I_{si} \cup I_{se}\}$ is the number of equilibrium reactions and $N_{rk} = \text{card}\{I_{sk}\}$ is the number of kinetic reactions such that $N_{re} + N_{rk} = N_r$.

The chemical system can be written as:

$$\sum_{j=1}^{N_c} \nu_{ij} A_j = 0, \quad i = 1, \ldots, N_r,$$

where ν_{ij} is the stoichiometric coefficient of the component A_j in the reaction i.

2.1.1 Equilibrium reactions

Each equilibrium reaction gives rise to an algebraic relation called mass action law, relating the activities of the components involved in the reaction:

$$a_\alpha^j = K_j \prod_{i \in I_p} (a_\alpha^i)^{\nu_{ji}}, \ j \in I_{sm} \cup I_{si}, \tag{1}$$

where a_α^j is the activity of component j in its phase α, K_j is the equilibrium constant of reaction j. The activity depends on the type of components and is often represented by the fugacity for gaseous species [35].

For each solid species involved in an equilibrium dissolution/precipitation reaction, a solubility product must be respected:

$$\begin{aligned} &\text{if } K_j \prod_{i \in I_p} (a_\alpha^i)^{\nu_{ji}} < 1 \text{ then } c_s^j = 0, \\ &\text{else } K_j \prod_{i \in I_p} (a_\alpha^i)^{\nu_{ji}} = 1, \ j \in I_{se}, \end{aligned} \tag{2}$$

where c_s^j denotes the molar concentration of solid species j expressed in [mol.m^{-3} medium]. This complementarity problem is often reformulated as:

$$\min \left(c_s^j, 1 - K_j \prod_{i \in I_p} (a_\alpha^i)^{\nu_{ji}} \right) = 0. \tag{3}$$

2.1.2 Kinetic reactions

Each kinetic reaction leads to an ODE [9]:

$$\frac{dc_s^j}{dt} = -r_j, \ j \in I_{sk}, \tag{4}$$

where c_s^j denotes the concentration of the solid species j.

In Eq. 4, the reaction rate r_j depends on the activities of the components involved in the kinetic reaction. In this paper, we consider only kinetic mineral dissolution/precipitation reactions, for which the reaction rate r_j can be expressed as follows:

$$r_j = K_j^s A_j^s \left(1 - K_j \prod_{i \in I_p} (a_\alpha^i)^{\nu_{ji}} \right), \ j \in I_{sk}, \tag{5}$$

where K_j^s and A_j^s are respectively the kinetic rate constant [mol.m^{-2}.s^{-1}] and the reactive surface [m^2.m^{-3}] of component j.

2.2 Mathematical model for two-phase multicomponent flow with reactive transport

We define the phase-species correspondence by setting α_i to the index of the phase that contains species i. The general mass conservation equations for the primary species write [35]:

$$\begin{aligned} &\frac{\partial}{\partial t} \left(\phi S_{\alpha_i} c_{\alpha_i}^i + \sum_{j \in I_{sm}} \phi \nu_{ji} S_{\alpha_i} c_{\alpha_j}^j + \sum_{j \in I_s \setminus I_{sm}} \nu_{ji} c_s^j \right) \\ &+ L_{\alpha_i}(c_{\alpha_i}^i) + \sum_{j \in I_{sm}} \nu_{ji} L_{\alpha_j}(c_{\alpha_j}^j) = 0, \quad i \in I_{pm}, \end{aligned} \tag{6}$$

$$\frac{\partial}{\partial t} \left(c_s^i + \sum_{j \in I_{si}} \nu_{ji} c_s^j \right) = 0, \quad i \in I_{pi}, \tag{7}$$

where ϕ [-] is the porosity of the medium, S_{α_i} [-] denotes the saturation of the fluid phase α_i and $c^i_{\alpha_i}$ [mol.m^{-3}] is the molar concentration of the fluid species i in the phase α_i.

L_{α_i} is the advection-diffusion operator in the phase α_i given by $L_{\alpha_i}(c^i_{\alpha_i}) = \nabla\cdot(c^i_{\alpha_i}\vec{q}_{\alpha_i}) - \nabla\cdot(D_{\alpha_i}\nabla c^i_{\alpha_i})$, where $\vec{q}_{\alpha_i}$ [m.s^{-1}] is the Darcy-Muskat velocity of the fluid phase α_i, D_{α_i} [m^2.s^{-1}] denotes the dispersive-diffusive tensor in the fluid phase α_i.

The Darcy-Muskat velocity of the fluid phase α is expressed as follows:

$$\vec{q}_\alpha = -\frac{k_{r\alpha}(S_\alpha)}{\mu_\alpha}\mathbb{K}(\nabla P_\alpha - \rho_\alpha^{mass}\vec{g}), \tag{8}$$

where $k_{r\alpha}$ [-] denotes the relative permeability of the fluid phase α, μ_α [Pa.s] is the dynamic viscosity of the fluid phase α, $\mathbb{K}$ [m^2] is the absolute permeability tensor, P_α [Pa] is the pressure of the fluid phase α and $\vec{g}$ [m.s^{-2}] is the gravitational acceleration.

Using the Millington and Quirk model, the dispersive-diffusive tensor in the fluid phase α writes:

$$D_\alpha = \phi^{\frac{4}{3}} S_\alpha^{\frac{10}{3}} D_{m,\alpha}\mathbb{I} + d_L|\vec{q}_\alpha|\mathbb{I} + (d_L - d_T)\frac{\vec{q}_\alpha\vec{q}_\alpha^T}{|\vec{q}_\alpha|}, \tag{9}$$

where $D_{m,\alpha}$ [m^2.s^{-1}] is the molecular diffusion in the phase α, d_L [m] and d_T [m] are the magnitudes of longitudinal and transverse dispersion respectively.

The phase pressures are connected by the capillary pressure law $P_c(S_{aq}) = P_g - P_{aq}$.

This system Eqs. 6–7 consisting of N_p degenerate PDEs is coupled with card$\{I_{sm}\cup I_{si}\}$ algebraic Eq. 1, card$\{I_{se}\}$ complementarity problems Eq. 3 and card$\{I_{sk}\}$ ODEs Eq. 4.

Let us end this section by the following remark. There exist several formulations of the above system that differ from each other by the number and type of unknowns. In the following, we will use the DSA formulation which presents a concise and general mathematical formulation for reactive multiphase flows in porous media.

3 Numerical scheme

In this section, we provide a description of our fully implicit strategy and its discretization using a conservative FV method. We first describe the formulation and derivation, followed by the FV scheme.

3.1 DSA formulation of the system

In this subsection, we present the DSA formulation of the coupled two-phase flow and geochemical model described in the previous section and that will be used in the sequel.

The DSA consists of replacing the concentrations of secondary species present in the mass balance Eqs. 6–7 by the expression $c^j_{\alpha_j} \overset{\text{def}}{=} \mathbb{C}^j_{\alpha_j}(\mathbf{c_p})$. $\mathbb{C}^j_{\alpha_j}$ is a function obtained using the mass action laws and $\mathbf{c_p} = (c^i_{\alpha_i})_{i\in I_p}$ is a vector containing the concentrations of all primary species. This method has the merit of reducing the number of unknowns compared to other formulations at the cost of having to solve a very strongly nonlinear system requiring the development of complex and adapted numerical strategies. The new set of equations becomes:

$$\begin{aligned}
&\frac{\partial}{\partial t}\left(\phi S_{\alpha_i}c^i_{\alpha_i} + \sum_{j\in I_{sm}}\phi\nu_{ji}S_{\alpha_i}\mathbb{C}^j_{\alpha_j}(\mathbf{c_p}) + \sum_{j\in I_s\setminus I_{sm}}\nu_{ji}\mathbb{C}^j_s(\mathbf{c_p})\right) + L_{\alpha_i}(c^i_{\alpha_i})\\
&+\sum_{j\in I_{sm}}\nu_{ji}L_{\alpha_j}(\mathbb{C}^j_{\alpha_j}(\mathbf{c_p})) = 0, \quad i\in I_{pm},
\end{aligned} \tag{10}$$

$$\frac{\partial}{\partial t}\left(c^i_s + \sum_{j\in I_{si}}\nu_{ji}\mathbb{C}^j_s(\mathbf{c_p})\right) = 0, \quad i\in I_{pi}, \tag{11}$$

$$\min\left(c^j_s, 1 - K_j\prod_{i\in I_p}(a^i_{\alpha_i})^{\nu_{ji}}\right) = 0, \quad j\in I_{se}, \tag{12}$$

$$\frac{dc^j_s}{dt} = -K^s_jA^s_j\left(1 - K_j\prod_{i\in I_p}(a^i_{\alpha_i})^{\nu_{ji}}\right), \quad j\in I_{sk}. \tag{13}$$

3.2 Finite volume discretization of two-phase compositional reactive flow

The spatial discretization of the strongly coupled system Eqs. 10–13, subject to boundary and initial conditions, employs a conservative FV method. For the sake of simplicity of exposition, here we present the scheme for a regular mesh. The extension to unstructured grids is straightforward. More precisely, the system Eqs. 10–13 is discretized using a cell-centered FV method. Figure 1 represents structured and unstructured grids admissible for Two-Point Flux Approximation Scheme (TPFA) [17]. For general grids, we employ a multi-point flux approximation (MPFA) scheme for the formulation of the discrete fluxes, which has been presented in [1] for 2D and [2] for 3D simulations.

The cell-centered FV method consists of integrating the Eqs. 10-13 on a control volume V_k and evaluating the fluxes at the interface γ_{kl} between two neighbouring elements V_k and V_l. We denote by $f_k = \frac{1}{|V_k|}\int_{V_k} f\,dV$ the average of a function f on each element V_k. By using the implicit Euler scheme for the time discretization and due to the fact that the approximation of the primary unknowns and the physical parameters are constant on each element V_k, the cell-centered FV scheme corresponding to the discretization of the equations is given by:

$$\frac{|V_k|}{\Delta t^n}\left(\left\{\phi S_{\alpha_i} c^i_{\alpha_i}\right\}^{n+1}_k - \left\{\phi S_{\alpha_i} c^i_{\alpha_i}\right\}^{n}_k\right) + \sum_{j\in I_{sm}} v_{ji}\frac{|V_k|}{\Delta t^n}\left(\left\{\phi S_{\alpha_j}\mathbb{C}^j_{\alpha_j}(\mathbf{c_p})\right\}^{n+1}_k - \left\{\phi S_{\alpha_j}\mathbb{C}^j_{\alpha_j}(\mathbf{c_p})\right\}^{n}_k\right)$$
$$+ \sum_{j\in I_s\setminus I_{sm}} v_{ji}\frac{|V_k|}{\Delta t^n}\left(\left\{\mathbb{C}^j_s(\mathbf{c_p})\right\}^{n+1}_k - \left\{\mathbb{C}^j_s(\mathbf{c_p})\right\}^{n}_k\right) + \sum_{l\in V(k)}|\gamma_{kl}|\left(\left\{c^i_{\alpha_i}\right\}^{n+1}_{kl}\left\{\vec{q}_{\alpha_i}\right\}^{n+1}_{kl} - \left\{D_{\alpha_i}\right\}^{n+1}_{kl}\left\{\nabla c^i_{\alpha_i}\right\}^{n+1}_{kl}\right)\cdot\vec{n}_{kl}$$
$$+ \sum_{j\in I_{sm}} v_{ji}\sum_{l\in V(k)}|\gamma_{kl}|\left(\left\{\mathbb{C}^j_{\alpha_j}(\mathbf{c_p})\right\}^{n+1}_{kl}\left\{\vec{q}_{\alpha_j}\right\}^{n+1}_{kl} - \left\{D_{\alpha_j}\right\}^{n+1}_{kl}\left\{\nabla\mathbb{C}^j_{\alpha_j}(\mathbf{c_p})\right\}^{n+1}_{kl}\right)\cdot\vec{n}_{kl} = 0, i\in I_{pm}, \tag{14}$$

$$\frac{|V_k|}{\Delta t^n}\left(\left\{c^i_s\right\}^{n+1}_k - \left\{c^i_s\right\}^{n}_k\right) + \sum_{j\in I_{si}} v_{ji}\frac{|V_k|}{\Delta t^n}\left(\left\{\mathbb{C}^j_s(\mathbf{c_p})\right\}^{n+1}_k - \left\{\mathbb{C}^j_s(\mathbf{c_p})\right\}^{n}_k\right) = 0, i\in I_{pi}, \tag{15}$$

$$\min\left(\{c^j_s\}^{n+1}_k, 1 - K_j\prod_{i\in I_p}\left\{(a^i_{\alpha_i})^{v_{ji}}\right\}^{n+1}_k\right) = 0,\ j\in I_{se}, \tag{16}$$

$$\left\{c^j_s\right\}^{n+1}_k = \left\{c^j_s\right\}^{n}_k - \Delta t^n K^s_j A^s_j\left(1 - K_j\prod_{i\in I_p}\left\{(a^i_{\alpha_i})^{v_{ji}}\right\}^{n+1}_k\right),\ j\in I_{sk}, \tag{17}$$

where Δt^n is the time step, $\vec{n}_{kl}$ denotes the unit outer normal to γ_{kl}, $V(k)$ is the set of adjacent elements of V_k. The discretization of the Darcy-Muskat velocity expresses as follows:

$$\left\{\vec{q}_\alpha\right\}^{n+1}_{kl} = -\left\{\mathbb{K}\right\}_{kl}\left\{\frac{k_{r\alpha}(S_\alpha)}{\mu_\alpha}\right\}^{n+1}_{kl}\left(\left\{\nabla P_\alpha\right\}^{n+1}_{kl} - \left\{\rho^{mass}_\alpha\right\}^{n+1}_{kl}\vec{g}\right).$$

Then, a fully upwinding scheme is used to approximate the numerical flux for the convective term. The quantities (S_α, $c^i_{\alpha_i}$, P_α and $k_{r\alpha}$) are evaluated implicitly and upstream at the interface γ_{kl} between two adjacent elements as:

$$\{\cdot\}^{n+1}_{kl} = \begin{cases}\{\cdot\}^{n+1}_k & \text{if}\quad \{\vec{q}_\alpha\}^{n+1}_{kl}\cdot\vec{n}_{kl} > 0,\\ \{\cdot\}^{n+1}_l & \text{else.}\end{cases} \tag{18}$$

The flux on the interfaces γ_{kl} are computed using a TPFA scheme, see for instance [17]. A harmonic average of the values between two adjacent elements is used to calculate the absolute permeability $\{\mathbb{K}\}_{kl}$ and the diffusion coefficients $\{D_\alpha\}^{n+1}_{kl}$ at the interface γ_{kl}. Finally, $\{\rho^{mass}_\alpha\}^{n+1}_{kl}$ is computed as the arithmetic average of two elements V_k and V_l.

Integrating the boundary and initial conditions into the FV discretization of system Eqs. 14–17 leads to a set of strongly nonlinear equations. In the next section, we describe the implementation of our strategy and its validation by examining several test cases.

4 Numerical results

The outline of this section is as follows. First, in Section 4.1, we present our implementation in the platform DuMu^X and a new local time stepping strategy for our fully implicit scheme. Our approach was validated by solving several tests in 1D and 2D, the numerical results were satisfactory and replicated to those in the literature. The results of these simulations are omitted since nothing startling was found. Instead, we concentrate on the results obtained in realistic two 3D test cases related to mineral trapping in the context of geological sequestration of CO_2. Modeling interactions

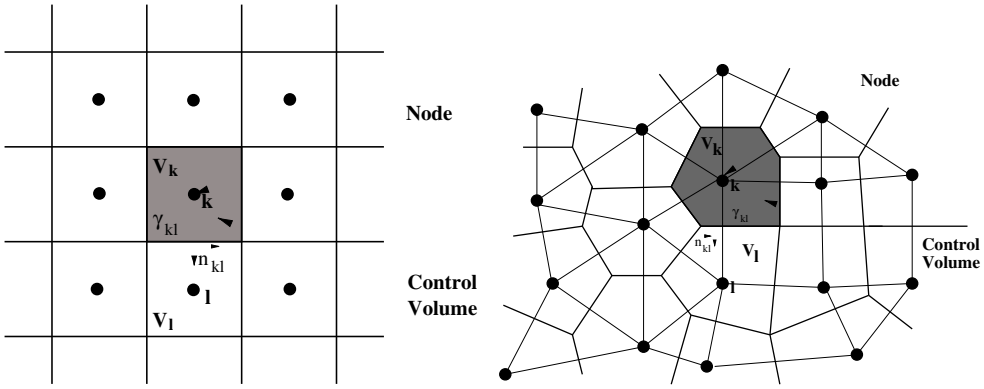

Fig. 1 Discretization by the cell-centered finite volume method: nodes and control volumes for structured (left) and unstructured meshes (right) admissible for TPFA

between CO_2 and mineral represents a crucial issue since mineral trapping of CO_2 is believed as the safest and the most permanent sequestration mechanism.

In Section 4.2, we present the numerical results obtained for an academic example proposed in [12] in which, the authors have used a global approach which is different from ours. This test aims at modeling the desired mechanisms by considering a chemical system involving three equilibrium precipitation-dissolution reactions. The configuration generates a precipitation-dissolution front. The evolution of gas saturation plus the concentrations of different species including minerals is illustrated and presents a good matching with the results obtained by the authors. We also provide an analysis of the nonlinear solver performance through the evolution of the time step and the number of Newton iterations during the simulation. Our numerical results on this test allow us to validate our approach with a comparison to a recent simulator and to offer a start of a benchmark with a comparative study with other teams.

Section 4.3 exhibits some numerical results obtained for a test case adapted from [18]. This test simulates precipitation-dissolution processes using kinetic reactions with strong chemical interactions. In addition to a numerical convergence study, the evolution of several quantities is exhibited and the distribution of CO_2 is also discussed in Section 4.3.1. Parallel scalability on modern computational platforms will be illustrated in Section 4.3.2 through strong and weak scaling studies, which will prove the efficiency of the proposed formulation in a parallel setting. Finally, in Section 4.3.3 we give an in-depth comparison of global and sequential approaches proposed in [4] within the same simulator, offering an opportunity to challenge the performance and accuracy of both approaches on a highly difficult 3D case. This allowed us to draw some interesting conclusions on the capabilities and benefits of the two methods on this type of test cases.

Both test cases show that our fully implicit approach is suitable to simulate strongly coupled multiphase flow and reactive transport problems.

4.1 Implementation

All our developments have been implemented in the free and opensource platform DuMu^X. It provides many tools to solve numerically PDEs and allowing, among other things, the management of mesh, discretization or linear and nonlinear solvers. The code is an object-oriented software written in C++ and has massively parallel computation capability. The modular concept of DuMu^X makes it easy to integrate new modules adapted to our numerical scheme.

Using the scheme as described above, we have developed a new module which allows to numerically solve the coupled system Eqs. 10–13 with a fully implicit scheme in time and a cell-centered FV method in space. We use Newton's method with variable time stepping. Numerical differentiation techniques are used to approximate the derivatives in the calculation of the Jacobian matrix. This allows to transform the nonlinear system of equations for each iteration step into a linear system of equations. For solving the occurring linearized systems of equations, an iterative linear solver is used, namely, BiConjugate Gradient STABilized (BiCGSTAB) method [31], preconditioned by an Algebraic Multigrid (AMG) solver [11]. This solver is integrated in the ISTL-Library of DUNE [10, 15].

The default time step strategy proposed in DuMu^X is based on the number of iterations required by Newton's method to achieve convergence for the last time iteration. The time step is reduced, if the number of iterations exceeds a specified threshold, whereas it is increased if the method converges within less iterations. Let us mention that throughout all 1D and 2D numerical experiments, we observed that a reasonable number of iterations was needed for the convergence of Newton's method. Consequently, for 1D and 2D problems the default strategy for the management of the time step may be sufficient.

However, for more complex 3D tests this default strategy leads to excessive CPU time. To overcome these challenges, we present a new local time stepping method for our fully implicit scheme. Our method, mainly heuristic, is based on an estimation parameter of the maximum normalized difference between solutions of two successive iterations for all variables. At the first Newton's iteration of each time iteration, this parameter can be used to evaluate the distance from the solution. For large parameter values, one can assume that the initial choice is quite far from the solution. We may then encounter difficulties for convergence or consume too much CPU time to converge. On the other hand, when this distance is small, we can afford to enlarge the time step by a certain factor depending not only on the number of Newton iterations but also on how small this parameter is. This indicator is also used in the strategy to proceed Newton iterations. If at the first Newton's iteration, this parameter is high, we assume that Newton's algorithm will probably diverge and we stop Newton iterations. With this strategy, we do not guarantee an unconditional convergence of Newton's method, but in return, we guarantee not to waste CPU time on Newton iterations that would probably not converge or in many iterations. The fully coupled fully implicit FV scheme, developed in this study, combined with time-accurate local time stepping allow Newton's method and linear solver to converge within a reasonable number of iterations which saves computing time. The modifications proposed allowed us to perform simulations faster than simulations using the default strategies by avoiding as much as possible unsuccessful Newton iterations. Let us briefly mention that various types of local time stepping strategies

for multiphase flow in porous media have been proposed in the literature, see for instance [26, 39] and the references therein.

Finally a remarkable property of the scheme is that the discrete maximum principles is satisfied which is crucial to obtain physically meaningful approximate solutions. This has been verified in all our simulations.

In view of the CPU times required for the examples treated in this paper, the new module developed is used on multicore / multinode systems. The parallelization in DuMu^X is carried out using the DUNE parallel library package based on MPI providing high parallel efficiency and allowing simulations with several tens of millions of degrees of freedom to be carried out, ideal for large-scale field applications. DuMu^X has the ability to run on anything from single processor systems to highly parallel supercomputers with specialized hardware architectures.

4.2 Test case 1

This test deals with a 3D simulation of injection of CO_2 into the subsurface. It has been proposed in [12] and it considers 5 equilibrium reactions presented in Table 1. Three minerals (Calcite, MinA, MinB) and seven aqueous reacting species are involved in these reactions. Calcite and MinB are carbonates while MinA is a silicate. The first reaction represents the interphase mass exchange of CO_2 between the gas and the aqueous phase that is modeled by the equation of state of Spycher and Pruess [34]. The second and third reactions allow the transformation of $CO_{2(aq)}$ into HCO_3^- and Calcite. These reactions increase the concentration of H^+ and MinA is dissolved and releases metal ions Me^{3+}. Finally, these ions Me^{3+} react with HCO_3^- to precipitate MinB.

For the last four reactions, the mass action laws are expressed in terms of concentrations:

$$\frac{c_{aq}^{HCO_3^-}\, c_{aq}^{H^+}}{c_{aq}^{CO_2}} = 10^{-3}, \qquad \frac{c_{aq}^{H^+}}{c_{aq}^{HCO_3^-}\, c_{aq}^{H^+}} = 1 \text{ if } c_s^{Calcite} > 0,$$

$$\frac{(c_{aq}^{H^+})^3}{c_{aq}^{Me^{3+}}\, c_{aq}^{SiO_2}} = 10^{-3} \text{ if } c_s^{MinA} > 0,$$

$$\frac{(c_{aq}^{H^+})^2}{c_{aq}^{HCO_3^-}\, c_{aq}^{Me^{3+}}} = 0.8 \text{ if } c_s^{MinB} > 0.$$

Table 1 Chemical reactions for test case 1

Reactions
$CO_{2(g)} \rightleftharpoons CO_2(aq)$
$CO_{2(aq)} + H_2O \rightleftharpoons H^+ + HCO_3^-$
$\text{Calcite} + H^+ \rightleftharpoons Ca^{2+} + HCO_3^-$
$\text{MinA} + 3H^+ \rightleftharpoons Me^{3+} + SiO_2$
$\text{MinB} + 2H^+ \rightleftharpoons Me^{3+} + HCO_3^-$

Figure 2 exhibits the computational domain. It is located 800 m below the surface, providing supercritical conditions for the CO_2. This latter is injected with a constant rate equal to 0.02 kg.m^{-2}.s^{-1} on Γ_{in} that corresponds to a square with side length 10 m. On Γ_D, Dirichlet boundary conditions corresponding to the initial values are enforced for pressure and concentrations. Impermeable Neumann boundary conditions are imposed on the remaining boundaries of the domain.

As initial conditions, hydrostatic condition is imposed for the pressure of aqueous phase P_{aq} and the domain is fully saturated by water ($S_{aq} = 1$). The initial concentrations and molar mass for each aqueous component are given in Table 2. Finally, the constitutive laws and physical parameters are given in Table 3.

The time of simulation is 85 days. We considered a grid composed of 40960 elements using the DUNE-ALUGrid module [7]. Figure 3 represents the time step used during the computations and the number of iterations in Newton's algorithm. It corresponds to 1686 time steps and an average number of $6-7$ iterations in Newton's algorithm per time step. Moreover, the maximum time step size $\Delta t_{max} = 5000s$ was employed. The numerical results are displayed in Figs. 4, 5 and 6 corresponding respectively to a time span of 7, 20 and 85 days. As expected, after the injection, the gaseous CO_2 rises to the top of the domain and accumulates. It is dissolved in the aqueous phase and the $CO_{2(aq)}$ reacts with water to release H^+. Due to the decrease of pH, Calcite and MinA are dissolved by the front of low pH water stream. Finally, the dissolution of MinA liberates ions Me^{+3}, inducing the precipitation of MinB. These results present a very good matching with those obtained by the authors.

This test case proves the ability of our fully implicit scheme to manage the appearance of the gas phase and to properly capture the propagation of the dissolution-precipitation front.

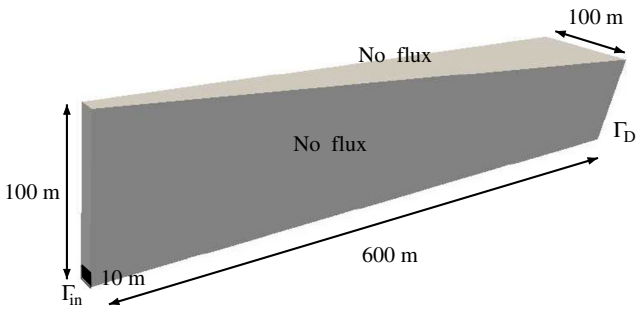

Fig. 2 Computational domain for test case 1

Table 2 Initial concentration and molar mass for test case 1

Component	Initial concentration [mol.m^{-3}]	Molar Mass [mol.kg^{-1}]
$CO_{2(aq)}$	10^{-2}	$4.4\,10^{-2}$
H_2O	55333.33	$1.8\,10^{-2}$
HCO_3^-	10^{-2}	$6.1\,10^{-2}$
H^+	10^{-3}	$1\,10^{-3}$
Ca^{2+}	10^{-1}	$4\,10^{-2}$
Me^{3+}	10^{-4}	$1.5\,10^{-2}$
SiO_2	10^{-2}	$6\,10^{-2}$
Calcite	0.1	–
MinA	0.2	–
MinB	0	–

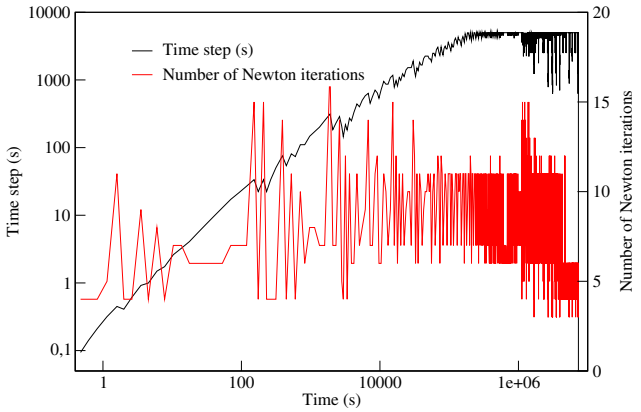

Fig. 3 Time step and number of iterations in Newton's algorithm versus time

4.3 Test case 2

4.3.1 Numerical simulations

This test concerns a 3D scenario of injection of CO_2 in a deep saline aquifer adapted from an example proposed in [18]. In addition to the validation of our fully implicit approach, this test case aims at providing a comparison between the fully implicit approach and the sequential strategy developed in [4].

The test case involves 7 reactions displayed in Table 4. The first four reactions are equilibrium reactions while the last three ones are kinetic and model mineral dissolution/precipitation processes. The first reaction expresses the phase equilibrium of CO_2 for which the solubility law is implemented according to [34]. Mineral data for the kinetic reactions such as the kinetic rate constant K^s and the reactive surface area A^s are summarized in Table 5.

The 3D domain is 15 km in both the x and y-directions and 100 m in the z-direction. A pure CO_2 stream is injected during the first 20 years through a well located 25 m from the top of the aquifer. After the 20 years injection period, a total of 18.6×10^9 kg of CO_2 has been injected. The duration of the simulation is 2000 years. As initial conditions, we used hydrostatic condition for the pressure of the aqueous phase P_{aq} and the initial saturation of the aqueous phase is set to $S_{aq} = 1$.

Table 3 Physical parameters for test case 1

Constitutive law or variable	Parameters
Porosity	$\phi = 0.2$
Absolute permeability	$\mathbb{K} = 10^{-12}\mathbb{I}$ m^2
Temperature	$T = 323\ K$
Brooks-Corey parameter	$S_{aq,r} = 0.2$, $S_{g,r} = 0.2$
Brooks-Corey parameter	$\lambda = 2$
Brooks-Corey parameter	$P_e = 1000$ Pa
Pure water mass density	$\rho_{aq}^{mass} = 992$ kg.m^{-3}
Aqueous molecular diffusivity	$D_{m,aq} = 0$ m^2.s^{-1}
Longitudinal dispersion coefficient	$\alpha_L = 0.1$ m
Longitudinal dispersion coefficient	$\alpha_T = 0.01$ m
Aqueous viscosity	$\mu_l = 6.526\ 10^{-4}$ Pa.s^{-1}

For the activity coefficients, the B-dot model is considered [23]:

$$\gamma^i = -\frac{Az_i\sqrt{I}}{1+\dot{A}_i B\sqrt{I}} + \dot{B}I, \tag{19}$$

where A, B and $\dot{B}$ are constants depending on the temperature, z_i is the ion electrical charge for species i and $\dot{A}_i$ is the ion size of species i. Finally, I is the ionic strength of the aqueous phase and expresses as $I = 0.5\sum_i m_l^i z_i^2$. Table 6 exhibits the parameters for the B-dot model.

The initial molalities and parameters for each ion are given in Table 7. Impermeable Neumann boundary conditions are enforced on the boundaries of the domain. Constitutive laws and physical parameters are given in Table 8.

Convergence analysis To validate our implementation, we conducted a numerical convergence study. Several cartesian structured meshes composed of 10 000, 80 000, 180 000 and 640 000 elements have been considered for this test case while a very fine mesh composed of 5.12×10^6 elements provided a reference solution. For each grid, we calculate h that represents the diagonal of the parallelepipedic cell.

Figure 7 represents the L^2 relative error between several variables and the reference solution as a function of'h on the whole domain at $t = 100$ years where a convergence phenomenon is observed. Most of the discretization schemes used are first order schemes in space, but except for calcite concentration where the order is close to one (1.07), the

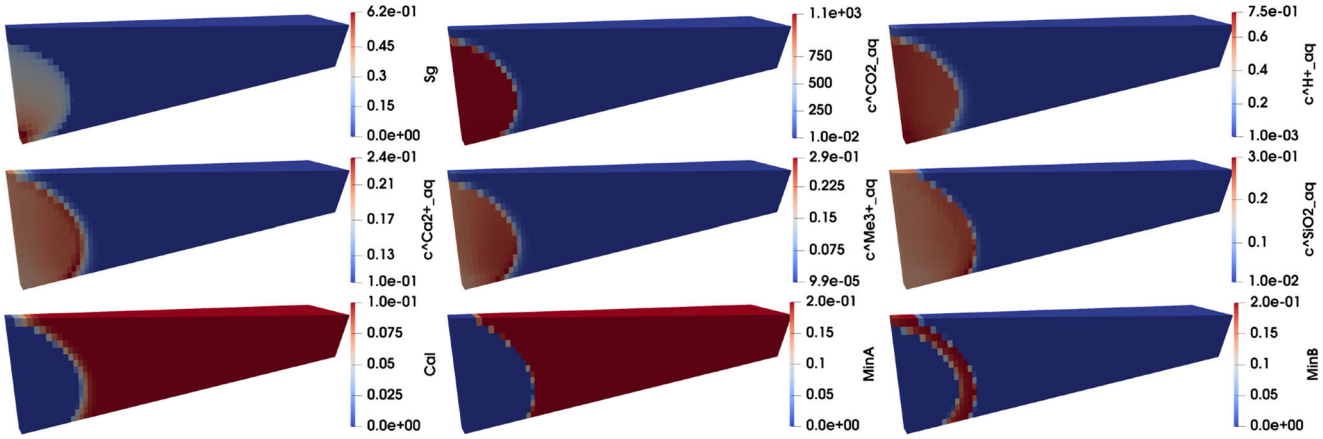

Fig. 4 Profiles for gas saturation and concentrations after 7 days for test case 1

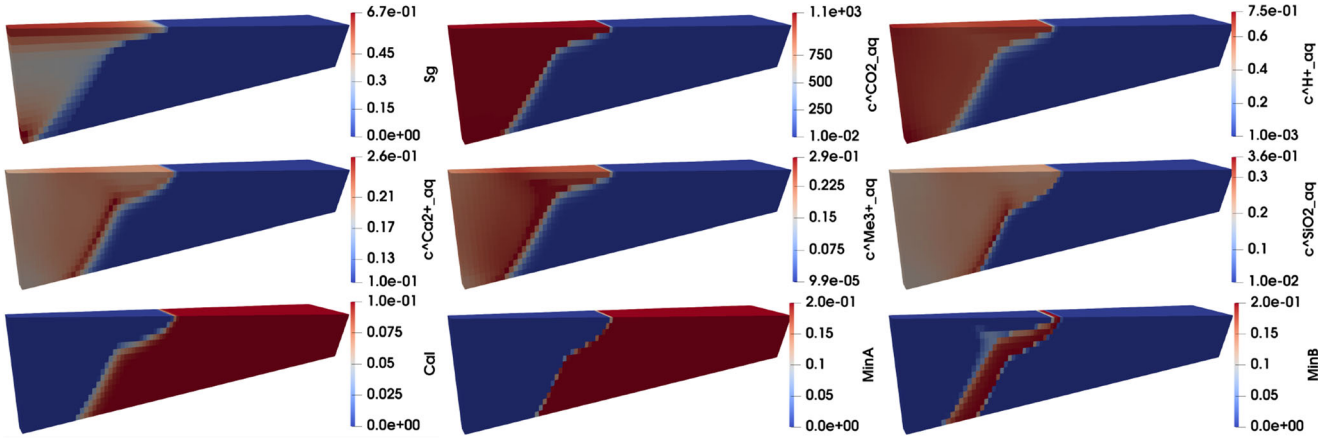

Fig. 5 Profiles for gas saturation and concentrations after 20 days for test case 1

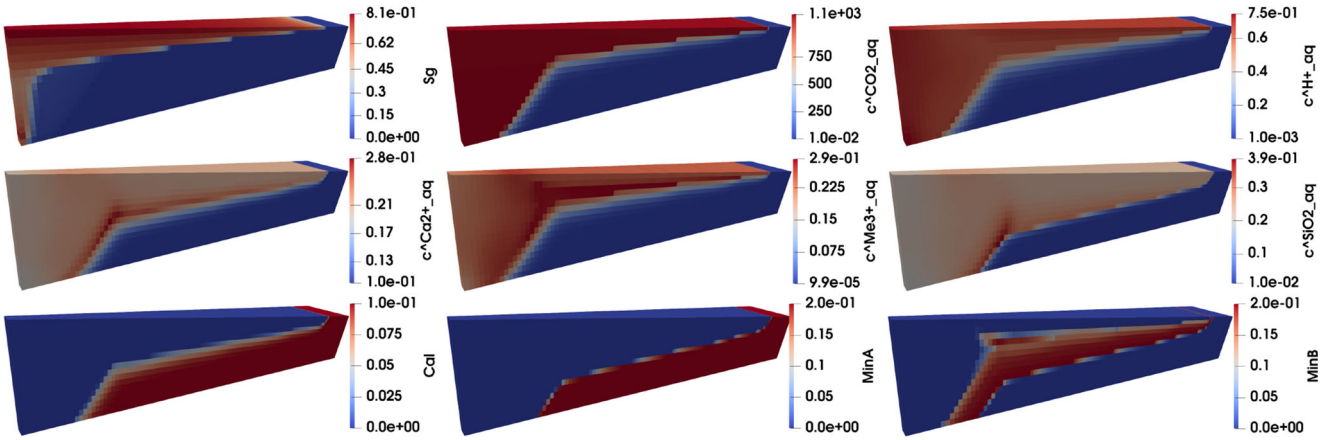

Fig. 6 Profiles for gas saturation and concentrations after 85 days for test case 1

Table 4 Chemical reactions for test case 2

Reactions	$log_{10}(K)$
$CO_{2(g)} \rightleftharpoons CO_{2(aq)}$	–
$CO_{2(aq)} + H_2O \rightleftharpoons H^+ + HCO_3^-$	–10.23
$CO_3^{2-} + H^+ \rightleftharpoons HCO_3^-$	–6.32
$OH^- + H^+ \rightleftharpoons H_2O$	–13.26
Anorthite $+ 8H^+ \rightleftharpoons 4H_2O +$ $Ca^{2+} + 2Al^{3+} + 2SiO_{2(aq)}$	25.82
Calcite $+ H^+ \rightleftharpoons Ca^{2+} + HCO_3^-$	1.6
Kaolinite $+ 6H^+ \rightleftharpoons 5H_2O + 2Al^{3+} + 2SiO_{2(aq)}$	6.82

Table 5 Mineral, precipitation and dissolution parameters for test case 2

Mineral	$log_{10}(K^s)$	A^s [$m^2.m^{-3}$]	Init. conc. [$mol.m^{-3}$]
Anorthite	–12.0	88	87
Calcite	–8.80	88	238
Kaolinite	–13.0	17600	88

Table 6 B-dot model parameters from the EQ3/6 database [40]

T (^oC)	25	60	100	150	200
A	0.4939	0.5465	0.5995	0.6855	0.7994
B	0.3253	0.3346	0.3421	0.3525	0.3639
$\dot{B}$	0.041	0.0438	0.046	0.047	0.047

Table 7 Input parameters for each ion for test case 2

Ion	Charge z	Size ($\dot{A}$)	Init. mol. [$mol.kg^{-1}$]
$CO_{2(aq)}$	0	3	3.55×10^{-3}
H^+	1	9	5.71×10^{-7}
Al^{3+}	3	9	3.13×10^{-12}
$SiO_{2(aq)}$	0	3	4.73×10^{-4}
Ca^{2+}	2	6	2.52×10^{-2}
HCO_3^-	–1	4.5	2.14×10^{-3}
CO_3^{2-}	–2	4.5	4.23×10^{-7}
OH^-	–1	3.5	4.49×10^{-8}

Table 8 Physical parameters for test case 2

Constitutive law	Parameters
Capillary pressure law	$P_c = 0$ Pa
Absolute permeability	$\mathbb{K} = 10^{-13}\mathbb{I}$ m^2
Relative permeability	
$k_{r,aq} = (S^*_{aq})^4$	$S^*_{aq} = \frac{S_{aq}-S_{aq,r}}{1-S_{aq,r}}$
$k_{r,g} = 0.4(1 - S^*_{aq})^2(1 - (S^*_{aq})^2)$	$S_{aq,r} = 0.2$
Aqueous diffusion tensor	
$D_{aq} = D_m\mathbb{I}$	$D_m = 10^{-9}$ $m^2.s^{-1}$
Gas diffusion tensor	Model based on [42]
Porosity	$\phi = 0.18$
Temperature	$T = 323\ K$
Aqueous density	Model based on [3]
Aqueous viscosity	$\mu_l = 4.8\ 10^{-4}$ Pa.s^{-1}
Gas density	Model based on [38]
Gas viscosity	Model based on [19]

order is degraded for other quantities (0.64 for gas saturation, 0.84 for $CO_{2(aq)}$ molality and 0.81 for H^+ molality), given the complexity of the phenomena considered and their strong nonlinearity.

Figure 8 illustrates the evolution of the concentration of calcite, anorthite and kaolinite at $t = 20$ years and $t = 2000$ years in comparison with their initial values given in Table 5 on a grid composed of 3.2×10^5 elements ($100 \times 100 \times 32$). Calcite is dissolved close to the injection zone and precipitated elsewhere while anorthite and kaolinite are respectively dissolved and precipitated everywhere in the domain.

Figure 9 depicts the evolution of the molality of $CO_{2(aq)}$ in the aqueous phase, pH and the gas saturation at $t = 20$ years and $t = 2000$ years. The pH and the molality of $CO_{2(aq)}$ are closely related since a high concentration of $CO_{2(aq)}$ acidifies the aqueous phase in the vicinity of the injection well. When injection of the $CO_{2(g)}$ stops, the gas which is less dense than the aqueous phase, migrates upwards and when it reaches the impervious top of the aquifer it spreads laterally. Then, the gaseous $CO_{2(g)}$ is dissolved in the aqueous phase and the CO_2-laden aqueous phase becomes denser than the surrounding brine and fingering phenomena can be observed after 2000 years.

Figure 10a) represents the net changes of each mineral in the aquifer while Fig. 10b) shows the distribution of carbon over time. Table 9 summarizes the carbon distribution at the end of the simulation. At 20 years, the highest amount of CO_2 is included in the gas phase. After the end of the injection, this amount decreases with time as CO_2 dissolves in the aqueous phase and reacts with ions and minerals.

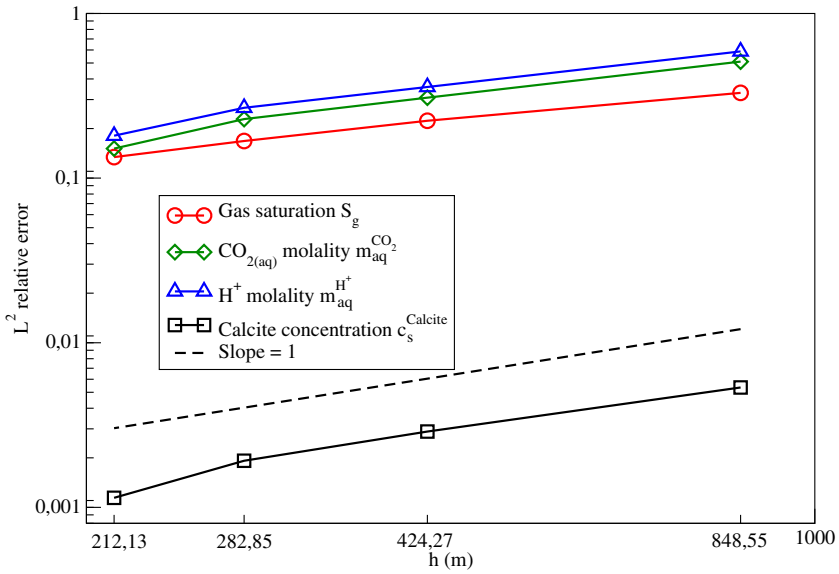

Fig. 7 Relative L^2 norm of the error S_g, $m_{aq}^{CO_2}$, $m_{aq}^{H^+}$ and $c_s^{Calcite}$ as a function of h at $t = 100$ years for test case 2

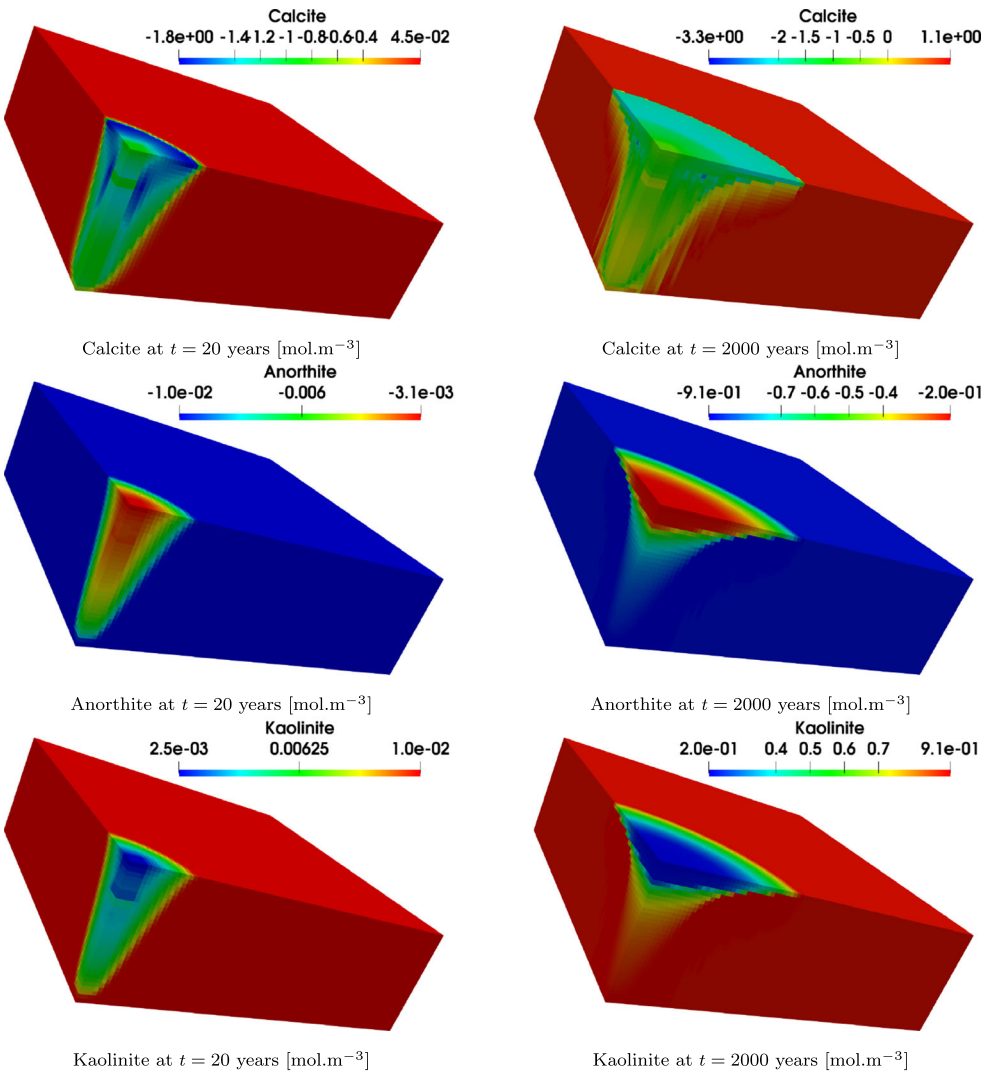

Calcite at $t = 20$ years [mol.m^{-3}]

Calcite at $t = 2000$ years [mol.m^{-3}]

Anorthite at $t = 20$ years [mol.m^{-3}]

Anorthite at $t = 2000$ years [mol.m^{-3}]

Kaolinite at $t = 20$ years [mol.m^{-3}]

Kaolinite at $t = 2000$ years [mol.m^{-3}]

Fig. 8 Evolution of the concentrations of minerals with respect to their initial values for test case 2. Positive and negative values indicate respectively precipitation and dissolution

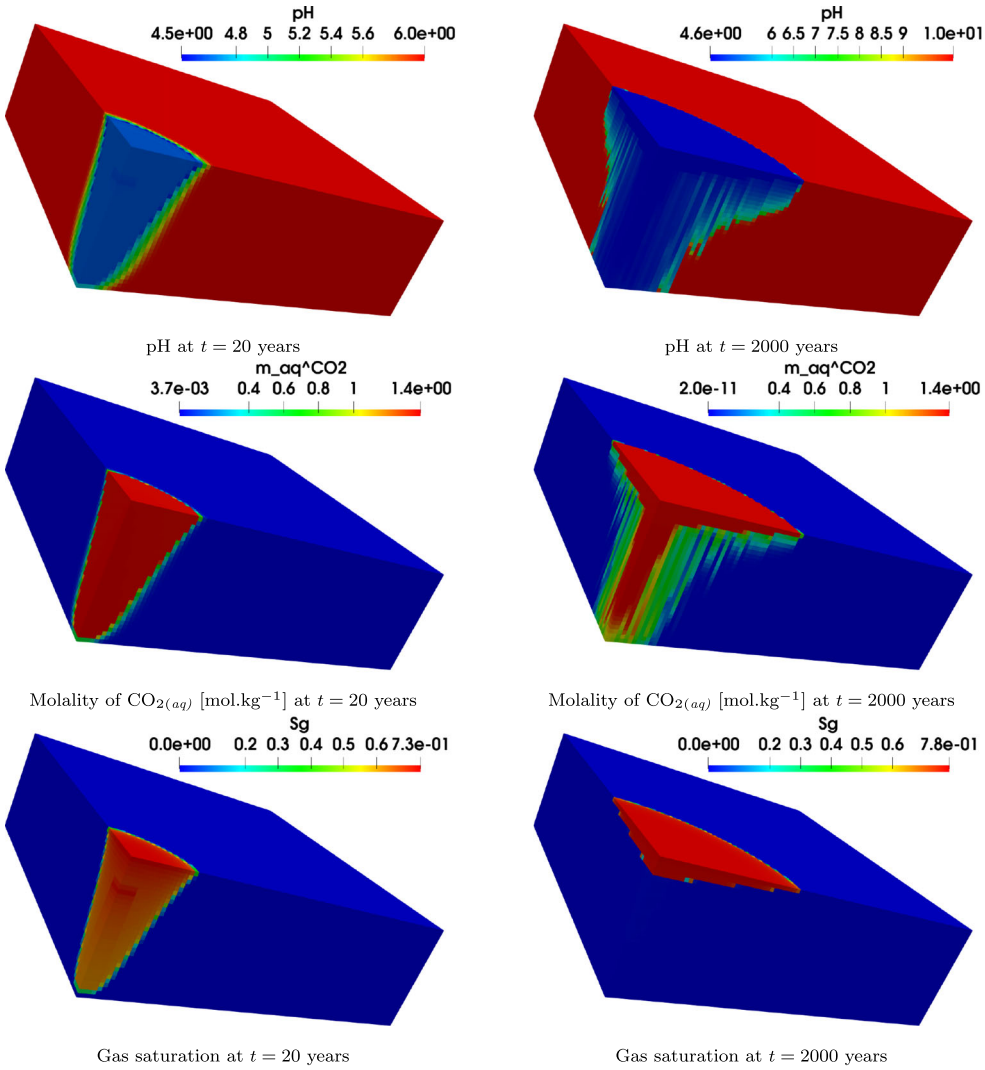

Fig. 9 Profiles for pH, molality of the aqueous $CO_{2(aq)}$ and gas saturation for test case 2

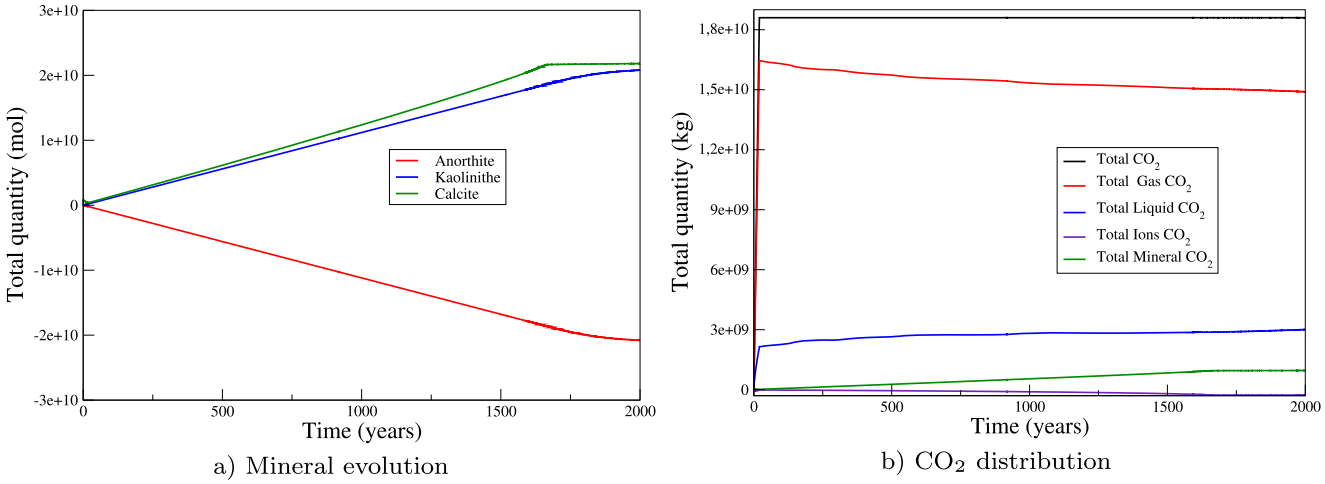

Fig. 10 Mineral net molar changes and evolution of CO_2 in time for test case 2

Table 9 Final carbon distribution at 2000 years for test case 2

In $CO_{2(g)}$	In $CO_{2(aq)}$	In ions	In minerals
80%	15.2%	0.5%	4.3%

In the aqueous phase, most of the carbon remains in the molecular form of $CO_{2(aq)}$ and only a negligible part of the carbon is stored in ionic form as HCO_3^- et CO_3^{2-} (0.5% at the end of the simulation). Mineralized carbon (in the form of calcite) accounts for 4.3% of the injected CO_2. These mineralization results are very strongly impacted by the reactive surface areas of minerals. Consequently, their computation remains a challenge.

4.3.2 High Performance Computing

DUNE provides arbitrary data decomposition in a generic way and the employed assembly operator and linear solvers are designed correspondingly. Parallel computations on a hierarchical grid follow the "single program multiple data" (SPMD) programming paradigm based on a suitable decomposition of the grid entities. Tasks are divided and run simultaneously on several processors with different input. Processors execute their own program and communicate with each other using the Message Passing Interface (MPI).

Parallel computations up to 768 processors have been performed on several grids. The parallel efficiency of our strategy is illustrated by solving 10 time steps. The code ran on a Bull cluster named OCCIGEN with Intel "Haswell" 12-Core E5-2690 V3 processors. In HPC, two types of scalability are defined. The first is the strong scaling, which represents the relation between the computational time and the number of processors for a fixed total problem size. The second is the weak scaling, for which the load per processor is fixed.

Strong scaling Figure 11a) depicts on a semi-logarithmic scale, CPU time as a function of the number of processors for 3 size problems of 640 000, 1.44×10^6 and 5.76×10^6 corresponding to approximately 5.76×10^6, 1.3×10^7 and 5.2×10^7 unknowns (there are 9 unknowns for each element).

The strong efficiency is given by:

$$S_e(N) = \frac{\text{CPU time on } p \text{ processors } \times p}{\text{CPU time on } N \text{ processors } \times N}, \tag{20}$$

here p denotes the number of processors used for the reference time (not necessary equal to one for heavy computations). For all calculations, we took $p = 48$. Strong efficiency reflects an optimal use of the parallel resources. An efficiency equal to one indicates that communications and synchronizations between processors using MPI protocol are negligible.

Figure 11b) represents the strong efficiency versus the number of processors. An excellent efficiency (greater than 0.90) is observed up to 192 processors for the computations involving 5.76×10^6 elements. The efficiency remains good (greater than 0.75) for the simulation with 1.44×10^6 elements up to 576 processors. For the simulation with 640 000 elements, efficiency is good (greater than 0.70) up to 192 processors. Beyond, the loss of efficiency is mainly due to the increase of the communications between processors in comparison with the load of each processor.

Weak scaling Figure 12a) displays CPU time as a function of the number of processors, with 3333, 10000 and 40000 elements per processor.

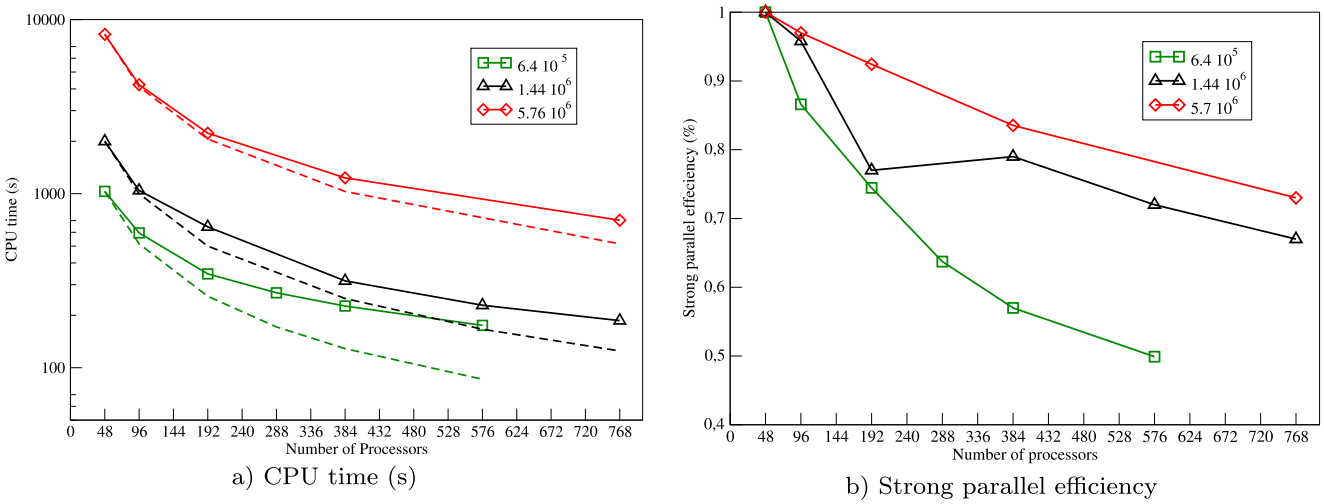

Fig. 11 CPU time (s) and strong parallel efficiency as a function of the number of processors for different problem sizes (the dashed lines represent an ideal behavior) for test case 2

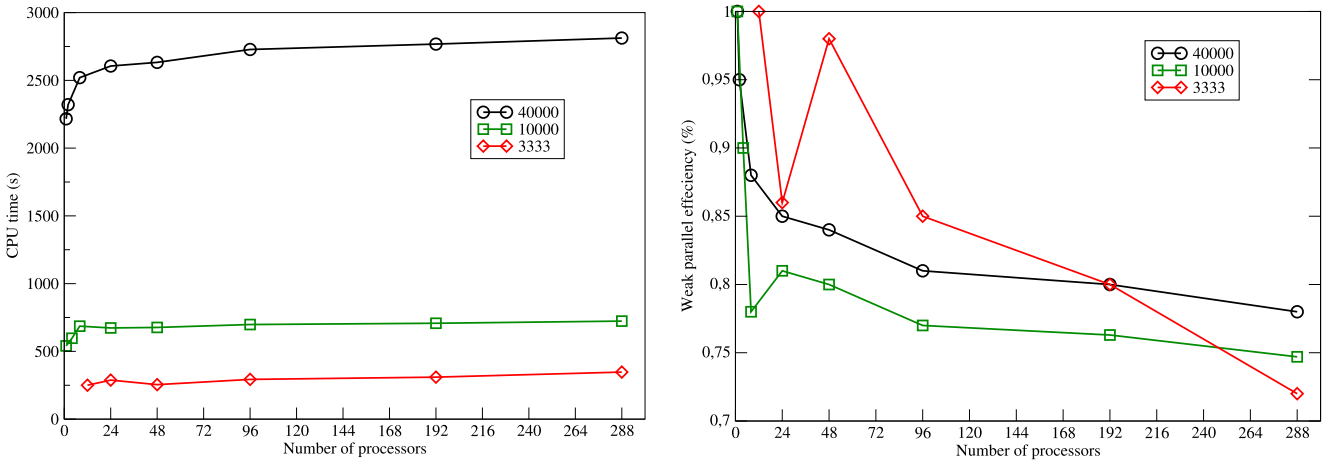

a) CPU time (s) b) Weak parallel efficiency

Fig. 12 CPU time (s) and weak parallel efficiency as a function of the number of processors for different problem sizes for test case 2

The weak efficiency is given by:

$$W_e(N) = \frac{\text{CPU time on } p \text{ processors}}{\text{CPU time on } N \text{ processors}}, \tag{21}$$

where p is defined in Eq. 20. Here, $p = 16$ for the scenario with 3333 elements per processor and $p = 1$ for the other two. An efficiency equal to one indicates an optimal behavior for the algorithm and the computer architecture. Indeed, CPU time remains constant, equal to the reference time, while the total size of the problem increases with the number of processors. Usually, this property is hardly verified as illustrated in Fig. 12b).

4.3.3 Comparison between fully implicit and sequential approaches

We propose here a comparison between the fully implicit and a sequential strategy developed in [4]. Table 10 presents the relative L^2 norm of the difference on the whole domain between the sequential and fully implicit solutions on different grids at $t = 20$ years. It confirms the closeness of the results since the highest gap is only few percents for the gas saturation and the molalities of $CO_{2(aq)}$ and H^+.

Carbon mass conservation To show the splitting errors induced by the sequential scheme, Figure 13 compares the evolution of the total mass of carbon for both sequential and fully implicit strategies with the exact quantity. Since the reservoir is closed, the exact quantity corresponds to the amount of injected CO_2. The injection rate is constant so during the first 20 years of simulations, the total mass of carbon grows with a linear rate and when the injection is cut off, this quantity stays constant. Figure 13 (left) compares both approaches during the first 30 years. The total mass of carbon increases linearly for both cases and is close to the exact quantity. The quantity reached at the end of the injection is very close for the two approaches. Figure 13 (right) represents the evolution from 20 years to 2000 years. The implicit strategy is fully mass conservative and the total mass of carbon keeps constant. Moreover, the quantity perfectly matches with the exact value. For the sequential approach, the quantity is not monotonous. Even if the gap between both approaches is rather small (only 1.3% at the

Table 10 Relative L^2 norm of the difference between several quantities computed by the fully implicit and sequential approaches for different meshes for test case 2 at $t = 20$ years

Mesh	320 000	180 000	80 000	10 000
S_g	$3.28\,10^{-3}$	$2.81\,10^{-3}$	$2.29\,10^{-3}$	$5.03\,10^{-3}$
P_{aq}	$1.04\,10^{-2}$	$1.05\,10^{-2}$	$1.06\,10^{-2}$	$1.12\,10^{-2}$
$CO_{2(aq)}$ molality	$1.75\,10^{-2}$	$1.74\,10^{-2}$	$1.70\,10^{-2}$	$1.40\,10^{-2}$
H^+ molality	$8.43\,10^{-2}$	$8.29\,10^{-2}$	$8.03\,10^{-2}$	$7.19\,10^{-2}$
Calcite concentration	$1.30\,10^{-4}$	$1.31\,10^{-4}$	$1.29\,10^{-4}$	$1.29\,10^{-4}$
Anorthite concentration	$1.14\,10^{-7}$	$9.08\,10^{-8}$	$7.66\,10^{-8}$	$6.09\,10^{-8}$
Kaolinithe concentration	$1.97\,10^{-7}$	$9.84\,10^{-8}$	$1.16\,10^{-7}$	$1.10\,10^{-7}$

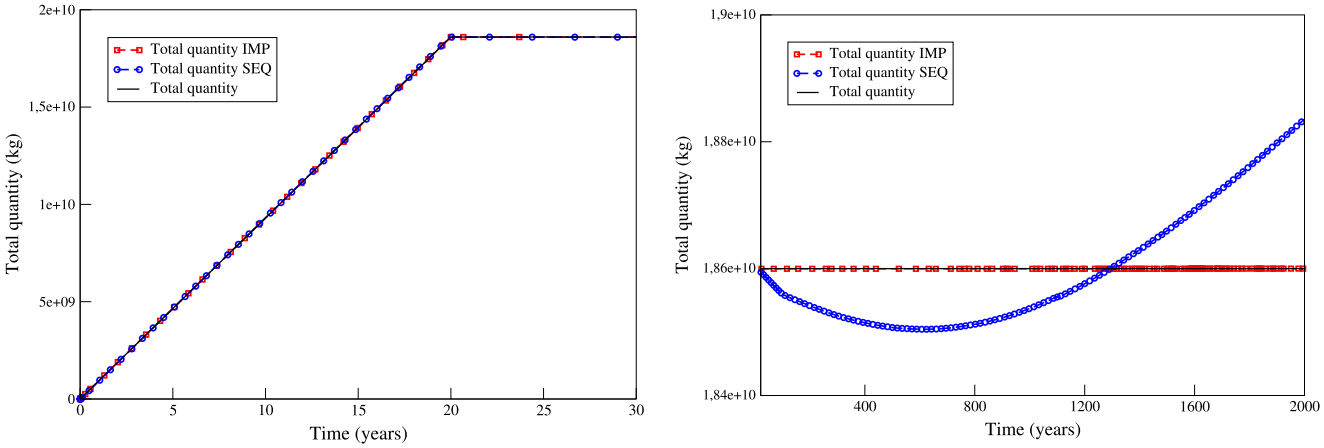

Fig. 13 Comparison of the total mass of carbon during the first 30 years (left) and from 20 years to 2000 years (right) for the sequential and implicit schemes

end of the simulation), the errors of splitting would be probably larger when simulating faster kinetics or stronger chemical interactions.

5 Conclusion and perspectives

In this article, we have presented a mathematical formulation and finite volume approximation for a system of coupled PDEs and algebraic or ODEs modeling two-phase reactive flows in the subsurface. A fully implicit approach has been developed and implemented in the framework of the parallel open-source platform DuMu^X. Numerical results concerning scenarios of geological storage of CO_2 validated the method. A comparison between our fully implicit scheme and a sequential one developed in [4] was carried out in the same numerical environment: both approaches provided very close results. We were able to highlight a small discrepancy in the estimation of total carbon mass for the sequential case whereas the implicit approach is totally mass-conservative. The fully implicit approach is more CPU time consuming than the sequential one, but the calculation times remain of the same order of magnitude.

Now, we have to continue to validate our fully implicit approach by considering additional benchmarks and stronger chemical interactions with porosity/permeability changes induced by mineral precipitation/dissolution. In this regard, we would like to point out that we encountered difficulties to find reliable and well documented benchmarks. In many articles, some data are missing. We think that a complete documented benchmark for two-phase flow with reactive transport in porous media would be very useful for the community. It is why, a contribution on this important issue is in progress. As already mentioned, most of the presented results concern two-phase reactive flows but the platform we developed is able to treat a more complex flow by considering multiphase multicomponent reactive flows. Finally, to make the implicit approach even more competitive, further improvements must continue to be achieved. Due to the strong coupling between multiphase flow and reactive transport inducing strong nonlinearities in the global problem, particular attention should be paid to improve the convergence of linear solvers, or to achieve computational savings by stopping timely the linear and nonlinear solvers.

Acknowledgements This research has been partly supported by the Carnot Institute ISIFoR project (Institute for the sustainable engineering of fossil resources). This support is gratefully acknowledged. The authors gratefully thank the anonymous referees for their insightful comments and suggestions. We also thank Mustapha El Ossmani for his help during the development of our reactive transport module in DuMu^X and the CINES (National Computing Center for Higher Education) to give us access to their computing resources facility. This work was granted access to the HPC resources of CINES under the allocations A0060610019 and A0080610019 made by GENCI. Computer time for a part of this study was also provided by the computing facilities MCIA (Mésocentre de Calcul Intensif Aquitain) of the Université de Bordeaux and of the Université de Pau et des Pays de l'Adour.

References

1. Aavatsmark, I.: An introduction to multipoint flux approximations for quadrilateral grids. Comput. Geosci. **6**, 405–432 (2002)
2. Aavatsmark, I., Eigestad, G.T.: Numerical convergence of the MPFA O-method and U-method for general quadrilateral grids. Int. J. Numer. Methods Fluids **51**, 939–961 (2006)
3. Adams, J.J., Bachu, S.: Equations of state for basin geofluids: algorithm review and intercomparison for brines. Geofluids **2**, 257–271 (2002)
4. Ahusborde, E., Amaziane, A., El Ossmani, M.: Improvement of numerical approximation of coupled two-phase multicomponent flow with reactive geochemical transport in porous media. Oil Gas Sci. Technol. - Rev. IFP Energies Nouvelles **73**, 73 (2018)

5. Ahusborde, E., Amaziane, B., El Ossmani, M., Id Moulay, M.: Numerical modeling and simulation of fully coupled processes of reactive multiphase flow in porous media. J. Math. Study **52**, 359–377 (2019)
6. Amir, L., Kern, M.: Preconditioning a coupled model for reactive transport in porous media. Int. J. Numer. Anal. Model. **16**, 18–48 (2019)
7. Alkämper, M., Dedner, A., Klöfkorn, R., Nolte, M.: The DUNE-ALUGrid module. Arch. Numer. Softw. **4**, 1–28 (2016)
8. Barry, D.A., Miller, T., Culligan-Hensley, P.J.: Temporal discretisation errors in non-iterative split-operator approaches to solving chemical reaction/groundwater transport models. J. Contam. Hydrol. **22**, 1–17 (1996)
9. Bethke, C. Geochemical and Biogeochemicalreaction Modeling, 2nd edn. Cambridge University Press, Cambridge (2007)
10. Bastian, P., Blatt, M., Dedner, A., Dreier, N.A., Engwer, C., Fritze, R., Gräser, C., Kempf, D., Klöfkorn, R., Ohlberger, M., Sander, O.: The DUNE framework: basic concepts and recent developments. Comput. Math. Appl. **81**, 72–112 (2020)
11. Bastian, P., Blatt, M., Scheichl, R.: Algebraic multigrid for discontinuous galerkin discretizations of heterogeneous elliptic problems. Numer. Linear Algebra Appl. **2**, 367–388 (2012)
12. Brunner, F., Knabner, P.: A global implicit solver for miscible reactive multiphase multicomponent flow in porous media. Comput. Geosci. **23**, 127–148 (2019)
13. Carrayrou, J., Kern, M., Knabner, P.: Reactive transport benchmark of MoMaS. Comput. Geosci. **14**, 385–392 (2010)
14. DuMu^X: DUNE for Multi-{Phase, Component, Scale, Physics,...} flow and transport in porous media. http://www.dumux.org (2021)
15. DUNE: The distributed and unified numerics environment. http://www.dune-project.org (2021)
16. Erhel, J., Sabit, S.: Analysis of a global reactive transport model and results for the MoMaS benchmark. Math. Comput. Simul. **137**, 286–298 (2017)
17. Eymard, R., Gallouët, T., Guichard, C., Herbin, R., Masson, R.: TP or not TP, that is the question. Comput. Geosci. **18**, 285–296 (2014)
18. Fan, Y., Durlofsky, L.J., Tchelepi, H.A.: A fully-coupled flow-reactive-transport formulation based on element conservation, with application to CO_2 storage simulations. Adv. Water Resour. **42**, 47–61 (2012)
19. Fenghour, A., Wakeham, W.A., Vesovic, V.: The viscosity of carbon dioxide. J. Phys. Chem. Ref. Data **27**, 31–44 (1998)
20. Hammond, G.E., Valocchi, A.J., Lichtner, P.C.: Modeling multicomponent reactive transport on parallel computers using Jacobian-Free Newton Krylov with operator-split preconditioning. Dev. Water Sci. Elsevier **47**, 727–734 (2002)
21. Hoffmann, J., Kräutle, J., Knabner, P.: A parallel global-implicit 2-D solver for reactive transport problems in porous media based on a reduction scheme and its application to the MoMaS benchmark problem. Comput. Geosci. **14**, 421–433 (2010)
22. Kala, K., Voskov, D., Huzefa Ammiwala, M.: Parameterization of element balance formulation in reactive compositional flow and transport. Soc. Petroleum Eng. https://doi.org/10.2118/193898-MS (2019)
23. Kirkham, D.H., Helgeson, H.C., Flowers, G.C.: Theoretical prediction of the thermodynamic behavior of aqueous electrolytes by high pressures and temperatures: IV. Calculation of activity coefficients, osmotic coefficients, and apparent molal and standard and relative partial molal properties to 600^{o}C and 5 KB. Am. J. Sci. **281**, 1249–1516 (1981)
24. Koch, T., Gläser, D., Weishaupt, K., Ackermann, S., Beck, M., Becker, B., Burbulla, S., Class, H., Coltman, E., Emmert, S., Fetzer, T., Grüninger, C., Heck, K., Hommel, J., Kurz, T., Lipp, M., Mohammadi, F., Scherrer, S., Schneider, M., Seitz, G., Stadler, L., Utz, M., Weinhardt, F., Flemisch, B.: DuMu^X 3 - an open-source simulator for solving flow and transport problems in porous media with a focus on model coupling. Comput. Math. Appl. **8**, 423–443 (2020)
25. Kräutle, S., Knabner, P.: A new numerical reduction scheme for fully coupled multicomponent transport-reaction problems in porous media. Water Resour. Res. **41**, W09414 (2005)
26. Linga, G., Møyner, O., Nilsen, H.M., Moncorgé, A., Lie, K.A.: An implicit local time stepping method based on cell reordering for multiphase flow in porous media. J. Comput. Phy. X **6** (2020)
27. Mayer, K.U., Frind, E.O., Blowes, D.W.: Multicomponent reactive transport modeling in variably saturated porous media using a generalized formulation for kinetically controlled reactions. Water Resour. Res. **38**, 1–21 (2002)
28. Mayer, K.U., MacQuarrie, K.T.B.: Solution of the MoMaS reactive transport benchmark with MIN3P-model formulation and simulation results. Comput. Geosci. **14**, 405–419 (2010)
29. Nghiem, L., Sammon, P., Grabenstetter, J., Ohkuma, H.: Modeling CO_2 storage in aquifers with a fully-coupled geochemical EOS compositional simulator. Soc. Pet. Eng. SPE-89474-MS (2004)
30. Niemi, A., Bear, J., Bensabat, J.: Geological Storage of CO_2 in Deep Saline Formations. Springer, Berlin (2017)
31. Saad, Y. Iterative Methods for Sparse Linear Systems, 2nd edn. Society for Industrial and Applied Mathematics, Philadelphia (2003)
32. Seigneur, N., Lagneau, V., Corvisier, J., Dauzères, A.: Recoupling flow and chemistry in variably saturated reactive transport modelling - an algorithm to accurately couple the feedback of chemistry on water consumption, variable porosity and flow. Adv. Water Resour. **122**, 355–366 (2018)
33. Sin, I., Corvisier, J.: Multiphase multicomponent reactive transport and flow modeling. Rev. Mineral. Geochem. **85**, 143–195 (2019)
34. Spycher, N., Pruess, K.: CO_2-H_2O mixtures in the geological sequestration of CO_2. II. Partitioning in chloride brines at 12–100°C and up to 600 Bar. Geochim. Cosmochim. Acta **69**, 3309–3320 (2005)
35. Steefel, C.I., Appelo, C.A.J., Arora, B., Jacques, D., Kalbacher, T., Kolditz, O., Lagneau, V., Lichtner, P.C., Mayer, K.U., Meeussen, J.C.L., Molins, S., Moulton, D., Shao, H., Šimůnek, J., Spycher, N., Yabusaki, S.B., Yeh, G.T.: Reactive transport codes for subsurface environmental simulation. Comput. Geosci. **19**, 445–478 (2015)
36. Steefel, C.I., Lasaga, A.I.: A coupled model for transport of multiple chemical species and kinetic precipitation/dissolution reactions with application to reactive flow in single phase hydrothermal systems. Am. J. Sci. May **294**, 529–592 (1994)
37. Steefel, C.I., MacQuarrie, K.T.B.: Approaches to modeling of reactive transport in porous media. Rev. Mineral. **34**, 82–129 (1996)
38. Span, R., Wagner, W.: A new equation of state for carbon dioxide covering the fluid region from the triple-point temperature to 1100 K at pressures up to 800 MPa. J. Phys. Chem. Ref. Data **25**, 1–88 (1996)
39. Vohralik, M., Wheeler, M.F.: A posteriori error estimates, stopping criteria, and adaptivity for two-phase flows. Comput. Geosci. **17**, 789–812 (2013)
40. Wolery, T.J.: EQ3/6 software package for geochemical modeling of aqueous systems: Package overview and instal- lation guide

(version 8.0) Lawrence Livermore National Laboratory Report UCRL-MA-110662 PT I (1992)
41. Xiao, Y., Whitaker, F., Xu, T., Steefel, C. (eds.): Reactive Transport Modeling: Applications in Subsurface Energy and Environmental Problems. Wiley, Hoboken (2018)
42. Xu, B., Nagashima, K., DeSimone, J.M., Johnson, C.S.: Diffusion of water in liquid and supercritical carbon dioxide: an NMR study. J. Phys. Chem. A **107**, 1–3 (2003)
43. Zhang, F., Yeh, G.T., Parker, J.C.: Groundwater Reactive Transport Models. Bentham e–books, Sharjah (2012)